

Kinetic Theory for Residual Neural Networks

Michael Herty, Torsten Trimborn, Giuseppe Visconti

Institut für Geometrie und Praktische Mathematik (IGPM)

RWTH Aachen University

Templergraben 55, 52062 Aachen, Germany

June 13, 2022

Abstract

Deep residual neural networks are performing very well for many data science applications. We use kinetic theory to improve understanding of existing methods. A simplified residual neural network (SimResNet) model, in which each layer consists of one neuron per input dimension at most, is studied in the limit of infinitely many inputs. This leads to a Vlasov type equation for the distribution of data, and we analyze it with respect to sensitivities and steady states. In the simple case of a linear activation function we can study moment model properties for one-dimensional input data. Further, a modification of the microscopic dynamics leads to a Fokker-Planck type formulation of the SimResNet, in which the concept of network training is replaced by the task of fitting distributions. The performed analysis is validated by numerical simulations. In particular, results on clustering and regression problems are presented.

Mathematics Subject Classification (2010) 35Q20 (Boltzmann equation), 35Q84 (Fokker-Planck equation), 90C31 (Sensitivity, stability, parametric optimization), 92B20 (Neural networks, artificial life and related topics), 68T05 (Learning and adaptive systems)

Keywords Residual neural network, continuous limit, mean field equation, kinetic equation, machine learning application

1 Introduction

The use of machine learning algorithms has gained a lot of interest in the past decade [16, 17, 25, 44]. Besides the data science problems like clustering, regression, image recognition or pattern formation there are novel applications in the field of engineering as e.g. for production processes [27, 35, 37]. In this study we focus on deep residual neural networks (ResNet) which date back to the 1970s and have been heavily influenced by the pioneering work of Werbos [43]. ResNet have been successfully applied to a variety of applications such as image recognition [45], robotics [48] or classification tasks [7]. More recently, also applications to mathematical problems in numerical analysis [24, 31, 32, 41, 49] and optimal control [34] have been studied. However, we point-out that these contributions are usually aimed to use machine learning in a collaborative fashion.

A ResNet can be shortly summarized as follows: Given inputs, which are usually measurements, the ResNet propagates those to a final state using a precise dynamics which depends on some parameters. This final state is usually called output and solves a given machine learning task. The parameters of the ResNet are determined by solving an optimization procedure, called training, aimed to minimize a suitable distance between the output of the network and a given target. The parameters are distinguished as weights and biases. For the training of ResNets back-propagation algorithms based on stochastic gradient descent method [43] or Kalman filters [18, 42, 46] are frequently used.

The purpose of this work is to use kinetic theory in order to gain insights on properties of the dynamic of ResNet. There have been made several attempts to describe ResNet by differential equations [3, 22, 33]. For example in [33] the connection of deep convolution neural networks to partial differential equation (PDE) is derived. In [3] the time continuous version of a ResNet is studied and different temporal discretization schemes are discussed. There are also studies on application of kinetic methods to ResNet [1, 23, 36]. For example in [36] the authors consider the limit of infinitely many neurons and gradient steps in the case of one hidden layer. They are able to proof a central limit theorem and show that the fluctuations of the neural network at the mean field limit are normally distributed.

In this work, in contrast to [36], we do not consider the limit of infinitely many neurons. Instead we fix the number of neurons to the number of input features, and we call the resulting network simplified residual neural network (SimResNet). From another perspective, we can see a SimResNet as a ResNet with one neuron in each layer, and where the dimension of the neurons is prescribed by the dimension of the input data. Networks with a similar type of structure have been proved to satisfy the universal approximation theorem [21]. We derive the time continuous limit of the SimResNet model which leads to a possible large system of ODEs. We consider the mean field limit in the number of inputs (or measurements) deriving a hyperbolic Vlasov type PDE. Throughout this microscopic to kinetic limit process we assume that the bias and weights are optimized and given. The purpose of this approach is to analyze the forward propagation of the derived mean field neural network model with given weights and bias. In particular, we study moment model properties in the simple setting of a linear activation function and one-dimensional features of the input data, deriving conditions on parameters to solve certain aggregation or clustering phenomena. Furthermore, we compute steady states and perform a sensitivity analysis. The quantity of interest of the sensitivity analysis is an operator called loss function. With the help of the sensitivities we are able to deduce a novel forward algorithm for the bias and weights in the case of a change in the input or target distribution. This kind of forward algorithm is easier and computationally cheaper in comparison to standard back-propagation algorithms, and therefore can be of utmost advantage in real world applications. The robustness, in terms of perturbations in the input data, of the SimResNet and its mean field limit has been recently studied in [40] using spectral methods.

In addition we study Boltzmann type equations with noisy neural network dynamics as extension to the mean field formulation. This modeling step is motivated by stochastic neural networks with stochastic output layers which capture uncertainty over activations, see e.g. [9, 26, 39, 47]. Long time behavior of such Boltzmann type equations can be conveniently studied in the grazing limit regime which naturally leads to Fokker-Planck type equations where it is possible to obtain non trivial steady state distributions [29, 30, 38]. Also, the Fokker-Planck asymptotic allows to replace the concept of training with the task of fitting a distribution by imposing conditions on the parameters of the network and on the choice of the activation function.

The outline of the paper is as follows. In Section 2 we define the microscopic ResNet model and its time continuous limit. In Section 3 we introduce first the SimResNet, i.e. a ResNet with one neuron per layer, and then we derive the mean field neural network model. We investigate steady states, moment properties and perform sensitivity analysis. The corresponding Boltzmann type neural network model is presented in Section 4, with an asymptotic limit leading to a Fokker-Planck equation. We analyze the ability of the Fokker-Planck equation to describe given target distribution depending on the choice of parameters and activation functions. In Section 5 we conduct several numerical test cases which validate the previous analysis. Especially, we conduct two classical machine learning tasks, namely a clustering problem and a regression problem. We conclude the paper in Section 6 with a brief conclusion and an outlook on future research perspectives.

2 Time Continuous Residual Neural Network

We assume that the input signal consists of d features. A feature is one type of measured data as e.g. temperature of a tool, length or width of a vehicle, color intensity of pixels of an image.

Without loss of generality we assume that the value of each feature is one dimensional and thus the input signals are given by $\mathbf{x}_i(0) \in \mathbb{R}^d$, $i = 1, \dots, M$. Here, M denotes the number of measurements or input signals. In the following, we assume that the number of neurons is identical in each layer, corresponding to a fully connected ResNet. Namely, we consider L layers and in each layer the number of neurons is given by $\bar{N} := dN$, where N is the number of neurons for one feature. The microscopic model which defines the time evolution of the activation energy of each neuron $\mathbf{x}_i^k(t) \in \mathbb{R}^d$, $k = 1, \dots, N$, fixed input signal $\mathbf{x}_i(0) \in \mathbb{R}^d$ reads [12]:

$$\begin{cases} \mathbf{x}_i^k(t + \Delta t) = \mathbf{x}_i^k(t) + \Delta t \sigma \left(\frac{1}{dN} \sum_{j=1}^N \hat{\mathbf{w}}_{kj}(t) \mathbf{x}_i^j(t) + \mathbf{b}(t) \right), \\ \mathbf{x}_i^k(0) = \mathbf{x}_i(0) \end{cases}, \quad (1)$$

for each fixed $i = 1, \dots, M$ and $k = 1, \dots, N$. Here, $\hat{\mathbf{w}}_{k,j}(t) \in \mathbb{R}^{d \times d}$, $k = 1, \dots, N, j = 1, \dots, N$ are the weights and $\mathbf{b}(t) \in \mathbb{R}^d$ the bias, defining the parameters of the network to be optimized. Instead, $\sigma : \mathbb{R} \rightarrow \mathbb{R}$ denotes the activation function which is applied component wise. Examples of activation functions are the identity function $\sigma_I(x) = x$, the so-called ReLU function $\sigma_R(x) = \max\{0, x\}$, the sigmoid function $\sigma_S(x) = \frac{1}{1 + \exp(-x)}$ and the hyperbolic tangent function $\sigma_T(x) = \tanh(x)$.

In (1) we formulated a neural network by introducing a parameter $\Delta t \in \mathbb{R}^+$. In a classical ResNet $\Delta t = 1$. Here, instead, we introduce a time discretization concept which corresponds to the discrete structure of the layers. More precisely the time step $\Delta t > 0$ is defined as $\Delta t := \frac{T}{L}$, with $T > 0$ being a final time. In this way, and from now on, we see (1) as an explicit Euler discretization of an underlying time continuous model. A similar modeling interpretation has been introduced in [33].

A crucial part in applying a neural network is the training procedure. By training one aims to minimize the distance of the output of the neural network at some fixed time $T > 0$ to the target $\mathbf{h}_i \in \mathbb{R}^d$. Mathematically speaking one aims to solve the minimization problem

$$\min_{\mathbf{w}, \mathbf{b}} \|\mathbf{x}_i(T) - \mathbf{h}_i\|_2^2,$$

where we use the squared L^2 distance between the target and the output to defined the loss function, and where \mathbf{w} and \mathbf{b} are the collection of the parameters. Other choices are certainly possible [14]. The procedure can be computationally expensive on the given training set. Most famous examples of such an optimization are back-propagation algorithms based on stochastic gradient descent [11] or ensemble Kalman filters [18, 42, 46]. In the following we always assume that the bias and weights are given so that the neural network is already trained.

In the time continuous limit, which corresponds to $\Delta t \rightarrow 0$ and $L \rightarrow \infty$, (1) formally leads to

$$\begin{cases} \dot{\mathbf{x}}_i^k(t) = \sigma \left(\frac{1}{dN} \sum_{j=1}^N \hat{\mathbf{w}}_{kj}(t) \mathbf{x}_i^j(t) + \mathbf{b}(t) \right), \\ \mathbf{x}_i^k(0) = \mathbf{x}_i(0), \end{cases}, \quad (2)$$

for each fixed $i = 1, \dots, M$ and $k = 1, \dots, N$.

Existence and uniqueness of a solution is guaranteed as long the activation function σ satisfies a Lipschitz condition.

3 Mean Field Formulation of Residual Neural Networks with a Simplified Structure

In this section we derive a PDE model for the forward propagation of the time continuous formulation of a residual neural network under an assumption on the maximum number of neurons in each layer. Precisely, we follow a Liouville type approach in order to compute a mean field equation holding in the limit of infinitely many measurements.

3.1 Simplified Residual Neural Network

We work with the following assumption: each layer consists of a single neuron for each input feature or dimension. In other words, we consider $N = 1$. A similar structure has been already considered e.g. in [21] showing that the universal approximation theorem holds true. Under this hypothesis equation (2) becomes

$$\begin{cases} \dot{\mathbf{x}}_i(t) = \sigma\left(\frac{1}{d}\mathbf{w}(t) \mathbf{x}_i(t) + \mathbf{b}(t)\right), \\ \mathbf{x}_i(0) = \mathbf{x}_i(0), \end{cases} \quad (3)$$

for each fixed $i = 1, \dots, M$, and where $\mathbf{w}(t) \in \mathbb{R}^{d \times d}$. This simplification is not only beneficial for the kinetic formulation of a neural network but reduces also the complexity of a neural network drastically, especially the cost in the training stage. We refer to formulation (3) as Simplified Residual Neural Network (SimResNet). The performance of the SimResNet has been successfully investigated for an engineering application [8].

3.2 Mean Field Limit

We perform a mean field limit in the number of measurements M . In this regime the dynamic of (3) can be described by a hyperbolic Vlasov type PDE

$$\partial_t g(t, \mathbf{x}) + \nabla_{\mathbf{x}} \cdot \left(\sigma \left(\frac{1}{d} \mathbf{w}(t) \mathbf{x} + \mathbf{b}(t) \right) g(t, \mathbf{x}) \right) = 0 \quad (4)$$

for the evolution of the compactly supported probability distribution function $g : \mathbb{R}^+ \times \mathbb{R}^d \rightarrow \mathbb{R}$ with known and normalized initial condition

$$g(0, \mathbf{x}) = g_0(\mathbf{x}), \quad \int_{\mathbb{R}^d} g_0(\mathbf{x}) \, d\mathbf{x} = 1.$$

Observe that $g_0(\mathbf{x})$ corresponds to the distribution of the features of the measured input data and that (4) preserves the mass, i.e. $\int_{\mathbb{R}^d} g(t, \mathbf{x}) \, d\mathbf{x} = 1, \forall t > 0$. The derivation of (4) from (3) is classical and shortly summarized hereinafter. We define the empirical measure of the solution vector $\mathbf{X} = (\mathbf{x}_1, \dots, \mathbf{x}_M)^T \in \mathbb{R}^{dM}$ as

$$\mu_{\mathbf{X}}^M(t, \mathbf{x}) = \frac{1}{M} \sum_{k=1}^M \delta(\mathbf{x} - \mathbf{x}_k(t))$$

and use it to connect the solution of the large system for the particles, i.e. the neurons, to the PDE. In fact, a straightforward calculation shows that $\mu_{\mathbf{X}}^M(t, \mathbf{x})$ is a weak solution of the equation (4). We refer e.g. to [2, 10, 13] for further details.

Using rigorous arguments, based on Dobrushin inequality, it is possible to show that the empirical measure converges to the solution of the mean field equation when $M \rightarrow \infty$ in Wasserstein distance. Here, we follow the presentation in [10]. The convergence is obtained in the space of probability measures $\mathcal{P}(\mathbb{R}^d)$ using the 1-Wasserstein distance, which is defined as follows:

Definition 1. *Let μ and ν two probability measures on \mathbb{R}^d . Then the 1-Wasserstein distance is defined by*

$$W(\mu, \nu) := \inf_{\pi \in \mathcal{P}^*(\mu, \nu)} \int_{\mathbb{R}^d} \int_{\mathbb{R}^d} |\xi - \eta| d\pi(\xi, \eta), \quad (5)$$

where \mathcal{P}^* is the space of probability measures on $\mathbb{R}^d \times \mathbb{R}^d$ such that the marginals are μ and ν i.e.

$$\int_{\mathbb{R}^d} d\pi(\cdot, \eta) = d\mu(\cdot), \quad \int_{\mathbb{R}^d} d\pi(\xi, \cdot) = d\nu(\cdot)$$

Theorem 1. *We assume that the activation function σ of the microscopic system (3) is Lipschitz continuous with Lipschitz constant $C_L > 0$. Let $g_0(\mathbf{x})$, initial condition of (4), be a probability measure with finite first moment such that*

$$W(\mu_0^M, g_0) \rightarrow 0, \text{ as } M \rightarrow \infty.$$

Then the Dobrushin stability estimate

$$W(\mu^M(t), g(t)) \leq \exp(C_L t) W(\mu^M, g_0)$$

is satisfied and thus

$$W(\mu^M(t), g(t)) \rightarrow 0, \text{ as } M \rightarrow \infty.$$

For the detailed proof of the above result we refer e.g. to [10].

We stress the fact that the mean field interpretation of a neural network is reasonable when the number of measurements is very large. However, equation (4) provides only a statistical point of view of the neural network propagation, namely any information on the network output of a precised measurement is lost.

In the following we discuss solution properties of (4). If the flux function $F(t, \mathbf{x}, u) := u \sigma\left(\frac{1}{d} \mathbf{w}(t) \mathbf{x} + \mathbf{b}(t)\right)$ fulfills

$$\begin{aligned} F &\in C^2(\mathbb{R}_+ \times \mathbb{R}^d \times \mathbb{R}; \mathbb{R}) \\ \partial_u F &\in L^\infty(\mathbb{R}_+ \times \mathbb{R}^d \times \mathbb{R}; \mathbb{R}) \\ \partial_u \operatorname{div}_x(F) &\in L^\infty(\mathbb{R}_+ \times \mathbb{R}^d \times \mathbb{R}; \mathbb{R}) \end{aligned} \quad (6)$$

then the hyperbolic conservation law (4) admits a unique weak entropy solution in the sense of Krůzkov for initial data $g_0 \in L^\infty \cap L^1$, see [4], and can be solved pointwise by the method of characteristics. In particular, the following result characterizes the steady state solution of (4).

Proposition 1. *Let $g(t, \mathbf{x})$ be a compactly supported weak solution of the mean field equation (4). Consider the case of the identity activation function $\sigma_I(x) = x$ or the L^∞ hyperbolic tangent activation function $\sigma_T(x) = \tanh(x)$. Assume $\mathbf{b}^\infty = \lim_{t \rightarrow \infty} \mathbf{b}(t)$ and $\mathbf{w}^\infty = \lim_{t \rightarrow \infty} \mathbf{w}(t)$ exist and are finite. Then*

$$g_\infty(\mathbf{x}) = \delta(\mathbf{x} - \mathbf{y})$$

is a steady state solution of (4) in the sense of distributions provided that \mathbf{y} solves $\frac{1}{d} \mathbf{w}^\infty \mathbf{y} + \mathbf{b}^\infty = \mathbf{0}$.

Proof. For a test function $\phi(\mathbf{x}) \in C_0^\infty(\mathbb{R}^d)$ the steady state equation reads

$$\int \nabla_{\mathbf{x}} \phi(\mathbf{x}) \sigma\left(\frac{1}{d} \mathbf{w}^\infty \mathbf{x} + \mathbf{b}^\infty\right) g_\infty(\mathbf{x}) = 0. \quad (7)$$

If $g_\infty = \delta(\mathbf{x} - \mathbf{y})$ is a Dirac delta function located at \mathbf{y} , equation (7) is satisfied only if \mathbf{y} is the solution to the system $\frac{1}{d} \mathbf{w}^\infty \mathbf{y} + \mathbf{b}^\infty = \mathbf{0}$. \square

3.3 Moment Properties of the One Dimensional Mean Field Equation

In the case of one feature, i.e. $d = 1$, the mean field equation (4) reduces to

$$\partial_t g(t, x) + \partial_x (\sigma(w(t) x + b(t)) g(t, x)) = 0. \quad (8)$$

Our subsequent moment analysis is performed in this simple case.

We first define the k -th moment, $k \geq 0$, and variance of the probability distribution g by

$$m_k(t) := \int_{\mathbb{R}} x^k g(t, x) dx, \quad \mathbb{V}(t) = m_2(t) - (m_1(t))^2. \quad (9)$$

Clearly, the possibility to obtain a moment model is solely determined by the shape of the activation function $\sigma(\cdot)$.

In the following we aim to study some properties of the solution g with respect to characterizations of the functions w and b . The definition of these properties is based on the expected value and energy of the solution to the mean field equation, as specified below.

Definition 2. We say that the solution $g(t, y)$, $(t, y) \in \mathbb{R}^+ \times \mathbb{R}$, to equation (8) is characterized by

(i) energy bound if

$$m_2(0) > m_2(t),$$

holds at a fixed time t ;

(ii) energy decay if

$$m_2(t_1) > m_2(t_2),$$

holds for any $t_1 < t_2$, i.e. if the energy is decreasing with respect to time;

(iii) concentration if

$$\mathbb{V}(0) > \mathbb{V}(t),$$

holds at a fixed time t ;

(iv) aggregation if

$$\mathbb{V}(t_1) > \mathbb{V}(t_2),$$

holds for any $t_1 < t_2$, i.e. if the variance is decreasing with respect to time.

We observe that if the first moment is conserved in time, then definition of energy bound, i.e. (i), is equivalent to concentration, i.e. (iii), and definition of energy decay, i.e. (ii), is equivalent to aggregation, i.e. (iv). In terms of a residual neural network, satisfying concentration or aggregation phenomena means that we can recover output distributions with decreasing variance with respect to the input distribution. In fact, we again stress the fact that from a kinetic perspective we provide only a statistical description of the neural network dynamic.

3.3.1 The Case of the Identity Activation Function

A simple computation reveals that the 0-th moment is conserved, i.e. $m_0(t) = 1$ holds for all times $t \geq 0$, as we expect since (4) is a conservation law. Instead, for $k \geq 1$ the dynamic in time of the corresponding moment is prescribed by the following linear ordinary differential equation:

$$\frac{d}{dt} m_k(t) = k \left(w(t) m_k(t) + b(t) m_{k-1}(t) \right), \quad m_k(0) = m_k^0. \quad (10)$$

Notice that the k -th moment only depends on the $k-1$ -th moment. It is then possible to solve the moment equations iteratively with the help of the separation of variables formula obtaining

$$m_k(t) = \exp \left\{ k \int_0^t w(s) ds \right\} \left[m_k(0) + \int_0^t \exp \left\{ -k \int_0^s w(x) dx \right\} k b(s) m_{k-1}(s) ds \right]. \quad (11)$$

Let us define

$$\Phi_k(t) := k \int_0^t w(s) ds$$

and study conditions to observe phenomena described in Definition 2.

Proposition 2. Assume that the bias is identical to zero, namely $b(t) \equiv 0$, $\forall t \geq 0$. Then we obtain

(a) energy bound if $\Phi_1(t) < 0$ at a fixed time t ;

(b) energy decay if and only if $w(t) < 0$ for all $t > 0$;

(c) aggregation if and only if $\lim_{t \rightarrow \infty} \Phi_1(t) = -\infty$. In particular the steady state is distributed as a Dirac delta centered at $x = 0$.

Proof. If $b(t) \equiv 0$ then (11) simplifies to

$$m_k(t) = m_k(0) \exp\{\Phi_k(t)\} \quad (12)$$

and thus the first and the second moment are identical except the given initial conditions. Then we can easily apply the definitions of energy bound, energy decay and aggregation to prove the statement. \square

Corollary 1. *Assume that the bias is identical zero, namely $b(t) \equiv 0, \forall t \geq 0$. Then*

- (a) *if energy bound exists at a time t we have concentration;*
- (b) *if energy decay holds we have aggregation.*

Proof. We start proving the first statement. First we observe that (12) is still true, since by hypothesis we assume that the bias is zero. Due to the definition of concentration we need to verify that $\mathbb{V}(0) > \mathbb{V}(t)$ for a fixed time t . Using the definition of the variance, concentration is implied by

$$m_2(0) (1 - \exp(\Phi_2(t))) > m_1(0)^2 (1 - \exp(2\Phi_1(t))).$$

For the second part, we observe that aggregation phenomena is verified if $\mathbb{V}(t_1) > \mathbb{V}(t_2)$ for any $t_1 < t_2$. This is equivalent to

$$\begin{aligned} m_2(t_1) - m_1(t_1)^2 &> m_2(t_2) - m_1(t_2)^2 \\ \iff m_2(t_1) - m_2(t_2) &> (m_1(t_1) - m_1(t_2)) (m_1(t_1) + m_1(t_2)) \\ \iff m_2(t_1) &> m_1(t_1)^2. \end{aligned}$$

\square

The two previous results suggest that $b(t) \equiv 0$ is a condition which allows to solve clustering problems at the origin, independently on the initial first moment. Conservation of the first moment is guaranteed by choosing $b(t) := -w(t)m_1(t)$. See the following results.

Proposition 3. *Let the bias be $b(t) := -w(t)m_1(t), \forall t \geq 0$. Then the first moment m_1 is conserved in time and we obtain*

- (a) *energy bound if $\Phi_2(t) < 0$ at a fixed time t ;*
- (b) *aggregation phenomena if $w(t) < 0$ holds for all $t \geq 0$. In particular the steady state is distributed as a Dirac delta centered at $x = m_1(0)$.*

Proof. The solution formula for the second moment is

$$m_2(t) = \exp\{\Phi_2(t)\}(m_2(0) - m_1(0)^2) + m_1(0)^2 = \exp\{\Phi_2(t)\}\mathbb{V}(0) + m_1(0)^2.$$

Then we have energy bound if

$$\mathbb{V}(0) (\exp\{\Phi_2(t)\} - 1) < 0$$

which is satisfied assuming that $\Phi_2(t) < 0$ at a fixed time t . For the second statement we observe that delta aggregation is also implied by $\frac{d}{dt}\mathbb{V}(g(t)) < 0$, for all times. Or, equivalently, by $\frac{d}{dt}m_2(t) < 0$, for all times. We have

$$\frac{d}{dt}m_2(t) = w(t)\mathbb{V}(t) < 0$$

if and only if $w(t) < 0$ for all times. \square

We aim to discuss the impact of the variance on aggregation and concentration phenomena. This is especially interesting if we do not focus on the long time behavior but rather aim to know if $\mathbb{V}(T) \leq V$ for some tolerance $V > 0$ and time $T > 0$. In applications this level would be determined by the variance of the target distribution and allows, for instance, to avoid over-fitting phenomena.

Corollary 2. *If the bias is identical to zero, namely $b(t) \equiv 0, \forall t \geq 0$, then the energy at time $t > 0$ is below tolerance $V > 0$ if*

$$\Phi_2(t) < \ln \left(\frac{V}{m_2(0)} \right)$$

is satisfied. Instead, the variance is below the level $V > 0$ if

$$\Phi_2(t) < \ln \left(\frac{V}{\mathbb{V}(0)} \right)$$

holds.

Similarly, if the bias fulfills $b(t) := -w(t)m_1(t)$, then the energy at time $t > 0$ is below the level $V > 0$ if

$$\Phi_2(t) < \ln \left(\frac{V - m_1(0)^2}{\mathbb{V}(0)} \right)$$

is satisfied provided that $V > m_1(0)^2$ holds. Instead, the variance at time $t > 0$ is below the level $V > 0$ if

$$\Phi_2(t) < \ln \left(\frac{V}{\mathbb{V}(0)} \right)$$

is satisfied provided that $V > 0$ holds.

Remark 1. *In general it is not possible to obtain a closed moment model in the case of the sigmoid $\sigma_S(x)$ or hyperbolic tangent $\sigma_T(x)$ activation function. Nevertheless one might approximate both activation functions by the linear part of their series expansion:*

$$\sigma_S(x) \approx \frac{1}{2} + \frac{x}{4}, \quad \sigma_T(x) \approx x,$$

and apply similar analysis discussed above for the identity activation function.

Remark 2. *In the case of the ReLU activation function we decompose the moments $k \geq 1$ in two parts*

$$m_k(t) = \int_{\Omega^+(t)} x^k g(t, x) dx + \int_{\Omega^-(t)} x^k g(t, x) dx,$$

and we define

$$m_k^+(t) := \int_{\Omega^+(t)} x^k g(t, x) dx, \quad m_k^-(t) := \int_{\Omega^-(t)} x^k g(t, x) dx$$

where $\Omega^+(t) := \{x \in \mathbb{R} \mid x > -\frac{b(t)}{w(t)}\}$ and $\Omega^-(t) := \mathbb{R} \setminus \Omega^+(t)$.

Let us define $a(t) = -\frac{b(t)}{w(t)}$, then using the Leibniz integration rule we compute

$$\frac{d}{dt} m_k^-(t) = a(t)^k g(t, a(t)) \frac{d}{dt} a(t) \tag{13}$$

and

$$\frac{d}{dt} m_k^+(t) = -a(t)^k g(t, a(t)) \frac{d}{dt} a(t) + kw(t)m_k^+(t) + kb(t)m_{k-1}^+(t) \tag{14}$$

$$+ a(t)^{k+1} w(t) g(t, a(t)) + a(t)^k b(t) g(t, a(t)). \tag{15}$$

Consequently, the evolution equation for the k -th moment cannot be expressed by a closed formula since it depends on the partial moment on $\Omega^+(t)$ and boundary conditions:

$$\frac{d}{dt} m_k(t) = k(w(t)m_k^+(t) + b(t)m_{k-1}^+(t)) + a(t)^{k+1} w(t) g(t, a(t)) + a(t)^k b(t) g(t, a(t)). \tag{16}$$

In the case of constant weights and bias the equality $\dot{m}_k = \dot{m}_k^+$ holds. Notice also that the above discussion simplifies in the case of vanishing bias, and it becomes equivalent to the case when the activation function is the identity function. In fact, if $b(t) \equiv 0, \forall t \geq 0$, then the set Ω^+ switches to be $(-\infty, 0)$ or $(0, \infty)$, depending on the sign of the weight $w(t)$. Moreover, thanks to (13) we immediately obtain that $\frac{d}{dt} m_k^- \equiv 0$ holds true and thus $\frac{d}{dt} m_k(t) = \frac{d}{dt} m_k^+(t)$ is satisfied for all $t \geq 0$. Hence, the evolution equation (16) reduces to the case (10) and same computations can be performed.

3.4 Forward Training of Weights and Bias

We aim to derive a novel training algorithm for the weights and bias. Classical backpropagation algorithms used for retraining of NN suffer in real world application under the high computational costs. Therefore we derive a forward algorithm with the help of a sensitivity analysis. More precisely we define a loss function (or target function) coupled to our mean field PDE, which we aim to minimize. Thus, in our setting training of a the mean field ResNet boils down to an optimal control problem. Therefore, we utilize adjoint calculus in order to compute the sensitivities of the loss function (gradients of the loss function with respect to the weights and bias). We employ these sensitivities to derive a gradient type algorithm. This gradient algorithm is able to compute novel weights and bias in case of a perturbed target or new initial conditions. As stated before, the benefit of this algorithm is the possibility to avoid a retraining via backpropagation in case of perturbations.

The quantity of interest is the distance of function g at finite time T to the target distribution h . We assume the ResNet has been trained using the following loss function:

$$D(T; w, b, g_0) := \frac{1}{2} \int_{\mathbb{R}} |g(T, x) - h(x)|^2 dx. \quad (17)$$

Notice that the minimization of the (17) defines an optimal control problem:

$$\begin{aligned} & \arg \min_{w, b} D(T; w, b, g_0) \\ & \text{subject to } \partial_t g(t, x) + \partial_x (\sigma(w(t) x + b(t)) g(t, x)) = 0, \\ & \quad g(0, x) = g_0(x). \end{aligned}$$

We may expect that training was expensive and will not necessarily be done again if input or target changes. Therefore, it is of interest if the trained network (namely w and b) can be reused if h or g_0 changes. We propose to compute the corresponding sensitivities of D with respect to the weight and bias. This in turn can be used to apply a gradient step on (w, b) . We use adjoint calculus to adjust (w, b) to the modified (h, g_0) .

The formal Lagrangian reads

$$\begin{aligned} L(g, \lambda, w, b) = & D(T) - \int_0^T \int_{\mathbb{R}} g(t, x) (\partial_t \lambda(t, x) + \sigma(w x + b) \partial_x \lambda(t, x)) dx dt \\ & + \int_{\mathbb{R}} (\lambda(T, x) g(T, x) - \lambda(0, x) g(0, x)) dx \end{aligned}$$

with Lagrange multiplier $\lambda(t, x)$. The corresponding adjoint equation can be obtained from the functional derivative of the Lagrangian.

$$\begin{aligned} \partial_g L(g, \lambda, w, b)[\delta g] = & \int_{\mathbb{R}} |g(T, x) - h(x)| \delta g(T, x) dx - \int_0^T \int_{\mathbb{R}} \delta g (\partial_t \lambda(t, x) + \sigma(w x + b) \partial_x \lambda(t, x)) dt dx \\ & + \int_{\mathbb{R}} \lambda(T, x) \delta g(T, x) dx \end{aligned}$$

Algorithm 1 Forward update of weights and bias

- 1: Initially select optimized weights w, b ;
- 2: Update D by new initial data and target (g_0, h) ;
- 3: Choose a tolerance $tol > 0$;
- 4: **while** $|w^{k+1} - w^k| + |b^{k+1} - b^k| < tol$ **do**
- 5: Compute the new updates as

$$w^{k+1} = w^k - \gamma \int_{\mathbb{R}} g x \sigma' \partial_x(\lambda) dx$$
$$b^{k+1} = b^k - \gamma \int_{\mathbb{R}} g \sigma' \partial_x(\lambda) dx,$$

6: **end while**

Furthermore, we obtain the sensitivities as

$$\partial_w L(g, \lambda, w, b)[\delta w] = \int_0^T \delta w \int_{\mathbb{R}} g(t, x) x \sigma'(wx + b) \partial_x(\lambda) dt dx$$
$$\partial_b L(g, \lambda, w, b)[\delta b] = \int_0^T \delta b \int_{\mathbb{R}} g(t, x) \sigma'(wx + b) \partial_x(\lambda) dt dx.$$

Hence, the strong form of the formal first order optimality conditions are given by:

$$\begin{aligned} \partial_t \lambda(t, x) + \sigma(wx + b) \partial_x \lambda(t, x) &= 0 \\ \lambda(T, x) &= |g(T, x) - h(x)| \\ \partial_t g(t, x) + \partial_x(\sigma(wx + b) g(t, x)) &= 0 \\ g(0, x) &= g_0(x) \\ \int_{\mathbb{R}} g(t, x) x \sigma'(wx + b) \partial_x(\lambda) dx &= 0, \quad \forall t \in [0, T] \\ \int_{\mathbb{R}} g(t, x) \sigma'(wx + b) \partial_x(\lambda) dx &= 0, \quad \forall t \in [0, T] \end{aligned}$$

where $\sigma'(x)$ is the derivative of the activation function. It is assumed that σ is differentiable, i.e. $\sigma = \sigma_T$ or $\sigma = \sigma_S$. Adjustment of optimal weights and bias can be then obtained via gradient step. Thus, the update of weights and bias after a perturbation of (g_0, h) is summarized in Algorithm 1.

4 Boltzmann type Equations

In general, a mean field equation can be obtained as suitable asymptotic limit of a Boltzmann type space homogeneous kinetic equation. We show that this is true also for the mean field interpretation (4) of the neural networks (3) by suitably defining instantaneous microscopic interactions emerging from the continuous dynamics.

In particular, the case of one-dimensional feature can be derived from a linear Boltzmann type equation. In fact, the system of ODEs (3) can be recast as the following interaction rule:

$$x^* = x + \sigma(w(t) x + b(t)), \tag{18}$$

where, by kinetic terminology, x^* and x are the post- and pre-collision states, respectively. In fact, (18) can be obtained from (3) by explicit Euler discretization with time step $\Delta t = 1$. The corresponding weak form of the Boltzmann type equation reads

$$\frac{d}{dt} \int_{\mathbb{R}} \phi(x) g(t, x) dx = \frac{1}{\tau} \int_{\mathbb{R}} [\phi(x^*) - \phi(x)] g(t, x) dx \quad (19)$$

where τ represents the interaction rate and $\phi \in C_0^\infty(\mathbb{R})$ is a test function. In the present homogeneous setting, τ influences only the relaxation speed to equilibrium and thus, without loss of generality, in the following we take $\tau = 1$. Then, the one-dimensional Boltzmann type equation (19) leads to the one-dimensional mean field equation (8) by suitable scaling [29, 30, 38].

Remark 3. *In the two-dimensional case, we lead to a nonlinear Boltzmann space homogeneous type equation provided a suitable definition of binary dynamics between the neurons. In fact, we can interpret the microscopic ODE model (3) as the following binary interactions:*

$$\begin{aligned} x^* &= x + \sigma \left(\frac{w(t)x + \bar{v}(t)y}{2} + b(t) \right), \\ y^* &= y + \sigma \left(\frac{v(t)y + \bar{w}(t)x}{2} + d(t) \right). \end{aligned}$$

An advantage of the Boltzmann type description (19) is the possibility to study different asymptotic scales, in addition to the mean field one, which can lead to equations with non-trivial steady states that allows for an analytically characterization. In particular, we can introduce a different concept of training in which the choice of weights w , bias b and of the activation function may be obtained by fitting the target distribution.

In order to obtain non-trivial steady states of model (19) one may consider self-similar solutions [30]:

$$\bar{g}(t, x) = m_1(t)g(t, m_1(t) x).$$

In the the case of the identity activation function the first moment can be computed explicitly, as showed in Section 3.3, and a Fokker-Planck type asymptotic equation can be derived. However, in order to study steady-state profiles for arbitrary activation functions, we choose the following approach: we add noise to the microscopic interaction rule (18) and apply a grazing collision limit leading to a Fokker-Planck type equation.

4.1 Fokker-Planck Description of the Simplified Residual Neural Network

Let ϵ be a small parameter, weighting for the strength of the interactions. Modify the interaction (18) as

$$x^* = x + \epsilon \sigma(w(t)x + b(t)) + \sqrt{\epsilon} K(x) \eta, \quad (20)$$

where η is a random variable with mean zero and variance ν^2 , and $K(x)$ is a diffusion function. For $K(x) = 0$ (20) corresponds to (1) with $\epsilon = \Delta t$ and to (18) with $\epsilon = 1$. The introduction of noisy interactions as in (20) is motivated by the need of recovering a broader class of steady states, in addition to the trivial ones described by the mean field equation. From the view-point of neural networks, this modeling assumption is inspired by stochastic neural networks with stochastic output layers [9, 26, 39, 47]. In general, stochastic neural networks consider random variations into the network, and one way to model these variations is using stochastic output layers which capture uncertainty over activations. It has been observed that this approach is useful for the optimization procedure, since the random fluctuations allow to escape from local minima. In the same spirit, we modify the deterministic interactions (18) by describing layers with uncertainty about some state in its computation also in the forward propagation.

In the classical grazing collision limit $t = \epsilon t$, $\epsilon \rightarrow 0$, we recover the following Fokker-Planck equation for the scaled probability distribution g :

$$\partial_t g(t, x) + \partial_x [\mathcal{B}g(t, x) - \mathcal{D}\partial_x g(t, x)] = 0 \quad (21)$$

where we define the interaction operator \mathcal{B} and the diffusive operator \mathcal{D} as

$$\mathcal{B} = \sigma(w(t)x + b(t)) - \frac{\nu^2}{2}\partial_x K^2(x), \quad \mathcal{D} = \frac{\nu^2}{2}K^2(x).$$

As the mean field limit, the grazing collision limit is also obtained by classical arguments and computations. Namely, starting from the linear Boltzmann type equation (19) one introduces a second order Taylor expansion of $\phi(x^*)$ around x and studying the limit $\epsilon \rightarrow 0$ one gets (21).

The advantage in computing the grazing collision limit is that the classical integral formulation of the Boltzmann collision term is replaced by differential operators. This allows a simple analytical characterization of the steady state solution $g_\infty = g_\infty(x)$ of (21). Provided the target can be well fitted by a steady state distribution of the Fokker-Planck type equation, the weight, the bias and the activation function are immediately determined. This is a huge computational advantage in comparison the classical training of neural networks. In the following we present examples of distributions that can be fitted by the solution of (21) in the large time behavior, finding conditions on weight, bias and activation function.

4.1.1 Steady State Characterization

Steady state solution of the Fokker-Planck type equation (21) can be easily found as

$$g_\infty(x) = \frac{C}{K^2(x)} \exp\left(\int \frac{2\sigma(w_\infty x + b_\infty)}{\nu^2 K^2(x)} dx\right) \quad (22)$$

where the constant $C \in \mathbb{R}$ is determined by mass conservation, i.e. $\int_{\mathbb{R}} g_\infty(x) dx = 1$. The existence and explicit shape of the steady state is determined by the specific choice of activation function $\sigma(\cdot)$, diffusion function $K(\cdot)$ and parameters w_∞, b_∞ . We discuss below some typical cases.

If the target $h(x)$ is distributed as a Gaussian, then choosing $\sigma(x) = \sigma_I(x)$ and $K(x) = 1$ the steady state (22) yields a suitable approximation of $h(x)$. In fact, we obtain

$$g_\infty(x) = C \exp\left(\frac{w_\infty}{\nu^2} x^2 + 2\frac{b_\infty}{\nu^2} x\right),$$

which is a Gaussian provided that $w_\infty < 0$ and $b_\infty = 0$. Moreover, condition on mass conservation leads to

$$C = \frac{\sqrt{-\frac{w_\infty}{\nu^2}} \exp\left(\frac{b_\infty^2}{w_\infty \nu^2}\right)}{\sqrt{\pi}},$$

which is defined for $w_\infty < 0$.

If the target $h(x)$ is distributed as an inverse Gamma, then choosing $\sigma(x) = \sigma_I(x)$ and $K(x) = x$ the steady state (22) is given by

$$g_\infty(x) = \begin{cases} 0, & x \leq 0, \\ \frac{C}{x^{1+\mu}} \exp\left(\frac{\mu-1}{x} \frac{b_\infty}{w_\infty}\right), & x > 0, \end{cases}$$

with $\mu := 1 + \frac{2w_\infty}{\nu^2}$ and normalization constant

$$C = \frac{\left((1-\mu)\frac{w_\infty}{b_\infty}\right)^\mu}{\Gamma(\mu)},$$

where $\Gamma(\cdot)$ denotes the Gamma function. Notice that we have to assume that $w_\infty < 0$ and $b_\infty > 0$ hold in order to obtain a distribution.

Let $\sigma(x) = \sigma_R(x)$ and $K(x) = x$, and, without loss of generality, assume $w_\infty < 0$ so that σ_R is identical zero on the set $\Omega := \{x \in \mathbb{R} | x \geq -\frac{b_\infty}{w_\infty}\}$. The steady state on Ω is given by $g_\infty^\Omega = \frac{c}{x^2}, c > 0$ and can be extended on \mathbb{R} by the Pareto distribution:

$$g_\infty = \begin{cases} -\frac{b_\infty}{w_\infty} \frac{1}{x^2}, & x \geq -\frac{b_\infty}{w_\infty}, \\ 0, & x < -\frac{b_\infty}{w_\infty}. \end{cases}$$

As last example, we notice that if the activation and the diffusion function are chosen as

$$\sigma_N(x) := \left[\frac{1}{\delta} \left(\frac{x}{c} \right)^\delta - 1 \right] x, \quad 0 < \delta < 1, \quad c > 0, \quad K(x) = x,$$

respectively, then it is possible to obtain a generalized Gamma distribution as steady state. This specific model has been discussed in [6] and the exponential convergence of the solution to the steady state has been proven in [28]. This may motivate to choose the novel activation function $\sigma_N(\cdot)$ provided that the data is given by a generalized Gamma distribution.

5 Numerical Experiments

In this section we present two classical applications for machine learning algorithms, namely clustering and regression problem. Using these applications we validate the theoretical observations of the moment model analysis in Section 3.3. In addition we test the weight and bias update derived in the sensitivity analysis in Section 3.4. Finally, we show that the Fokker-Planck type interpretation of the neural network is able to fit non trivial continuous probability distributions. We point-out that the weights and bias we use for these experiments are assumed given and are constant in time. In fact, it is not the aim of this paper discussing training of parameters for the PDE versions of the neural network.

For the simulations we solve the PDEs models presented in this work by using a third order finite volume scheme [5], briefly reviewed below. All the cases we consider for the numerical experiments can be recast in the following compact formulation:

$$\partial_t u(t, x) + \partial_x F(u(t, x), t, x) = \frac{\nu^2}{2} \partial_{xx} u(t, x) + kS(u(t, x)), \quad (23)$$

with ν and k given constants. Application of the method of lines to (23) on discrete cells Ω_j leads to the coupled system of ODEs

$$\frac{d}{dt} \bar{U}_j(t) = -\frac{1}{\Delta x} [\mathcal{F}_{j+1/2}(t) - \mathcal{F}_{j-1/2}(t)] + \frac{\nu^2}{2} K_j(t) + kS_j(t), \quad (24)$$

where $\bar{U}_j(t)$ is the approximation of the cell average of the exact solution in the cell Ω_j at time t .

Here, $\mathcal{F}_{j+1/2}(t)$ approximates $F(u(t, x_{j+1/2}), t, x_{j+1/2})$ with suitable accuracy and is computed as a function of the boundary extrapolated data, i.e.

$$\mathcal{F}_{j+1/2}(t) = \mathcal{F}(U_{j+1/2}^+(t), U_{j+1/2}^-(t))$$

and \mathcal{F} is a consistent and monotone numerical flux, evaluated on two estimates of the solution at the cell interface, i.e. $U_{j+1/2}^\pm(t)$. We focus on the class of central schemes, in particular we consider a local Lax-Friedrichs flux. In order to construct a third-order scheme the values $U_{j+1/2}^\pm(t)$ at the cell boundaries are computed with the third-order CWENO reconstruction [5, 20].

The term $K_j(t)$ is a high-order approximation to the diffusion term in (23). In the examples below we use the explicit fourth-order central differencing employed in [19] for convective-diffusion

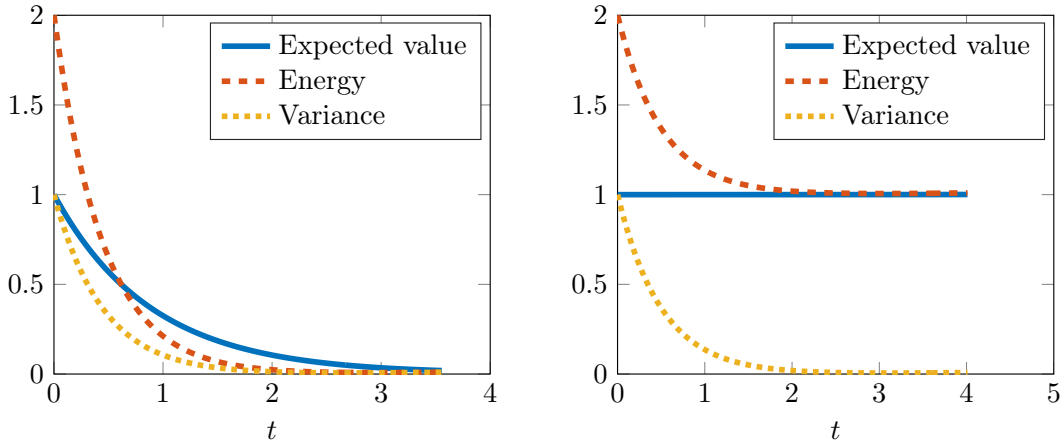


Figure 1: Left: Moments of our PDE model with $\sigma(x) = x, w = -1, b = 0$. Right: Moments of our PDE model with $\sigma(x) = x, w = -1, b = -\frac{m_1(t)}{m_0(0)}$.

equations with a general dissipation flux, and which uses point-values reconstructions computed with the CWENO polynomial.

Finally, $\mathcal{S}_j(t)$ is the numerical source term which is typically approximated as $\mathcal{S}_j(t) = \sum_{q=0}^{N_q} \omega_q S(\mathcal{R}_j(t, x_q))$, where x_q and ω_q are the nodes and weights of a quadrature formula on Ω_j . We employ three point Gaussian quadrature formula matching the order of the scheme.

System (23) is finally solved by the classical third-order (strong stability preserving) SSP Runge-Kutta with three stages [15]. At each Runge-Kutta stage, the cell averages are used to compute the reconstructions via the CWENO procedure and the boundary extrapolated data are fed into the local Lax-Friedrichs numerical flux. The initial data are computed with the three point Gaussian quadrature. The time step Δt is chosen in an adaptive fashion and all the simulations are run with a CFL of 0.45.

5.1 Moment Model Analysis Validation

In Section 3.3, thanks to the corresponding moment model, we have extensively discussed properties of the solution of the mean field limit of the SimResNet using a linear activation function. In this subsection we provide a numerical evidence of the theoretical findings by considering the following Gaussian probability distribution

$$g_0(x) = \frac{1}{\sqrt{2\pi}} \exp \left\{ -\frac{(x-1)^2}{2} \right\}$$

as initial condition of (8). This would represent, e.g., the distribution of given input data of a neural network.

As predicted by Proposition 1 a steady state of the mean field equation is a Dirac delta. Proposition 2 and Proposition 3 give conditions on the parameters to get a Dirac delta as output of the network. In particular, with the choice $w = -1, b = 0$ a decay to zero of the energy, expected value and the variance is expected and this is depicted in the left plot of Figure 1. Instead, choosing $b = -\frac{m_1(t)}{m_0(0)}$ guarantees conservation of the first moment as shown in the right plot of Figure 1.

Finally, Figure 2 illustrates the findings of Corollary 2. We compute the time needed in order to reach a fixed desired threshold of the energy and of the variance value. This means that, from a mean field view-point of a neural network, we can gain insights on the final time we consider in order to meet the variance of the target distribution, thus avoiding over-fitting phenomena.

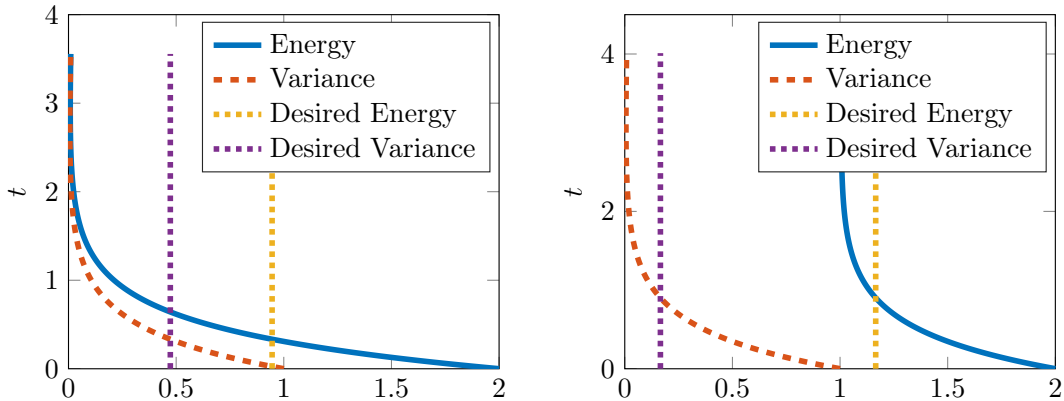


Figure 2: Left: The energy and variance plotted against the desired values with $\sigma(x) = x, w = -1, b = 0$. Right: The energy and variance plotted against the desired values with $\sigma(x) = x, w = -1, b = -\frac{m_1(t)}{m_0(0)}$.

5.2 Machine Learning Applications

We present here the experiments based on the kinetic approach, i.e. relying on the probabilistic interpretation, for the solution of classification and regression problems in machine learning. In all these simulations the activation function is chosen to be the hyperbolic tangent, i.e. $\sigma(x) = \sigma_T(x) = \tanh(x)$.

5.2.1 A Classification Problem

Consider a classification problem as follows. We measure a quantity (e.g. length of a car) and we need to identify the type of the object related to that measurement (e.g. car or truck). Therefore, in a classification problem, the task of the neural network is to determine the type given a measurement. Keeping in mind the example of identifying cars or trucks from their length measurement, a data set might look like Table 1 below, with a suitable scalar label for the classifiers.

Table 1: Example of input data.

Measurement	3	3.5	5.5	7	4.5	8	...
Classifier	car	car	truck	truck	car	truck	...

A probabilistic interpretation of the input data set can be obtained by considering the normalized histogram of the frequency of the given measurements, as in the left plot of Figure 3. In this example, the classifier is artificially associated to the binary values 2, for cars, and 8, for trucks. In terms of the kinetic interpretation, a continuous approximation of the histogram of input measurements is used as initial distribution of the mean field limit of the neural network model. Whereas, the output is expected to be Dirac delta distributions located at the chosen binary values distinguishing the classifier. In other words, the kinetic variable describes the distribution of the measurements, in this case the length of vehicles, at initial time. Instead, at final time, it represents the *mass* of identified cars and trucks.

On the particle level, cf. right plot of Figure 3, we observe the convergence in time of given measurements to the expected clusters. In this case a simple evolution of the time continuous microscopic model (3) is employed. For the evolution of the mean field equation, this type of experiment requires the introduction of zero flux boundary conditions on the numerical scheme.

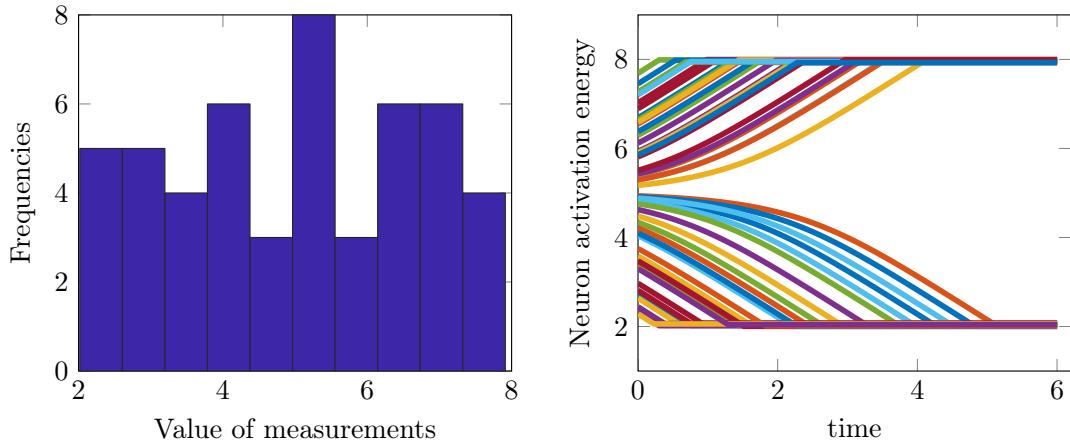


Figure 3: We consider 50 vehicles with measured length 2 and 8 obtained as uniformly distributed random realizations. Left: Histogram of the measured length of the vehicles. Right: Trajectories of the neuron activation energies of the 50 measurements.

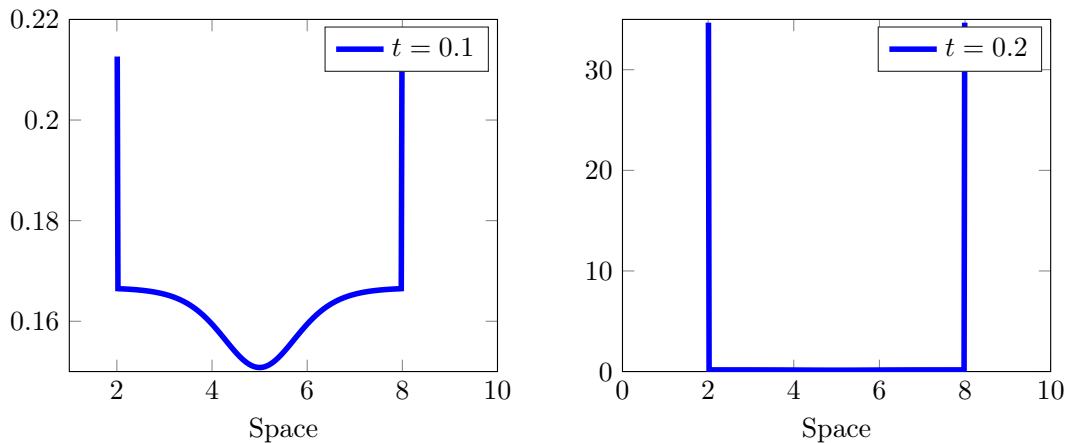


Figure 4: Solution of the mean field neural network model at different time steps. The initial value is a uniform distribution on $[2, 8]$ and the weight and bias is chosen as $w = 1$, $b = -5$.

The solution to the mean field interpretation of the neural network model is depicted in Figure 4 at different times.

Certainly, as already discussed, the mean field equation provides a good approximation of the microscopic dynamics when the number of input measurements is very large. However, due to the simplistic formulation of the classification problem we observe a good agreement of the results obtained at the discrete and and at the continuous level.

5.2.2 A Regression Problem

We may have given measurements at fixed locations. These measurements might be disturbed possibly due to measurement errors as in the left plot of Figure 5. In a regression problem the task of the neural network is to find a linear fit $y = mx + q$ of those data points, thus learning its

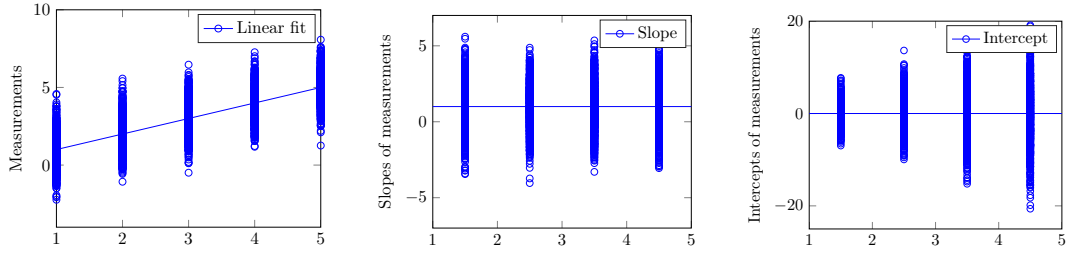


Figure 5: Left: Regression problem with $5 \cdot 10^3$ measurements at fixed positions around $y = x$. Measurement errors are distributed according to a standard Gaussian. Center: Numerical slopes computed out of the previous measurements. Right: Numerical intercepts computed out of the previous measurements.

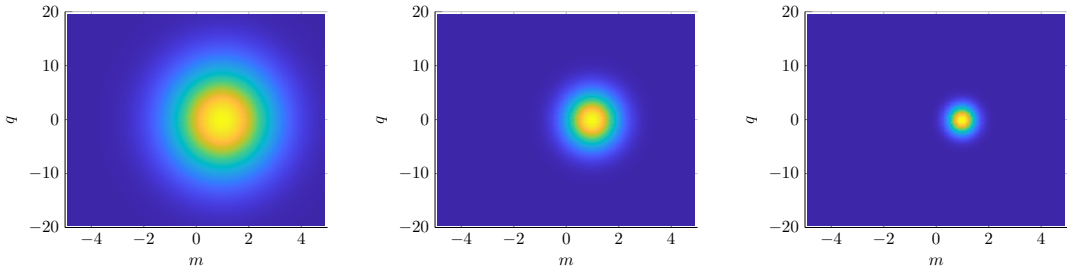


Figure 6: Evolution at time $t = 0$ (left plot), $t = 1$ (center plot), $t = 2$ (right plot) of the mean field neural network model (25) for the regression problem with weights $w_{xx} = 1$, $w_{xy} = w_{yx} = 0$, $w_{yy} = -1$, and bias $b_x = -1$, $b_y = 0$.

slope m and the vertical intercept q , i.e. the intersection of the linear function with the y axis. This type of problem can be reformulated in a two-dimensional setting, where the given measurements are used to generate an input data set of slopes and vertical intercepts, see the center and the right plots of Figure 5.

Also in this application we can build a probabilistic interpretation of the data set by considering the histogram of input data and its continuous approximation which is used as initial condition of the mean field limit equation (4). We point-out that in this example we need to consider the two dimensional version of the mean field PDE (4), namely

$$\partial_t g(t, x, y) + \partial_x \left(\frac{w_{xx}x + w_{xy}y}{2} + b_x \right) + \partial_y \left(\frac{w_{yx}x + w_{yy}y}{2} + b_y \right) = 0. \quad (25)$$

The solution of the mean field equation collapses to a Dirac delta distribution located at $(m, q) = (1, 0)$, as we expect to recover from the regression problem. See Figure 6. The parameters used to solve (25) are specified in the caption of Figure 6. Further, we employ the identity activation function and we again stress the fact that in this choice, as well as in the choice of the parameters, we are using the theoretical findings of the moment model analysis in Section 3.3.

5.3 Experiment on the Forward Training of Weights and Bias

We aim to present the benefit of the sensitivity analysis in Section 3.4 which has lead to a forward algorithm for the updates of weights and bias. To this end, we consider again a regression problem, with the same idea presented in the previous section. However, for simplicity and without loss of generality, we restrict the regression example to the one dimensional setting in which the task is learning the slope of the linear fit.

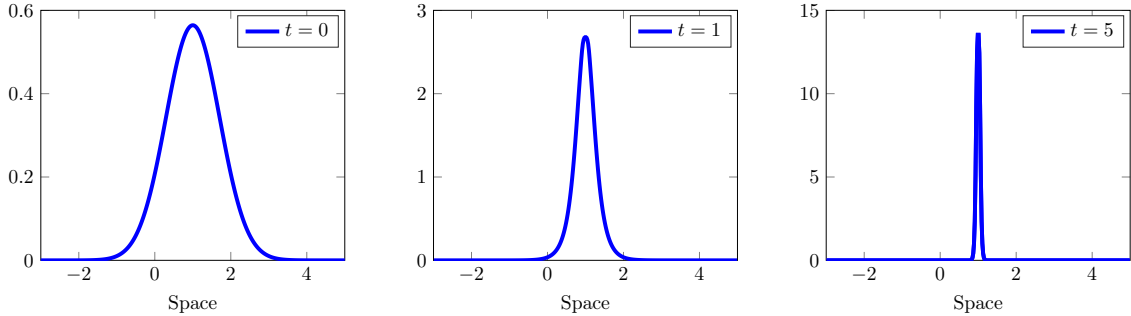


Figure 7: Evolution at time $t = 0$ (left plot), $t = 1$ (center plot), $t = 5$ (right plot) of the one dimensional mean field neural network model for the regression problem with weight $w = 1$ and bias $b = -1$.

The distribution of the input data is assumed to be a Gaussian with mean and variance equal to one, and the target distribution is a Dirac delta centered at location $x = 1$. The parameters of the mean field PDE, i.e. the weights and bias, are $w = 1$ and $b = -1$, respectively, as in the previous section. Therefore, the evolution of the one dimensional mean field equation can be observed in Figure 6 along the m direction, and depicted in Figure 7 for the sake of readability.

As Figure 6 shows, the solution at time $t = 5$, i.e. $g(t = 5, x)$, is close to the target which is a Dirac delta centered at $x = 1$. In order to investigate the application of the forward algorithm for the update of weight and bias, we consider a new target distribution, namely a Dirac delta centered at $x = 2$. In a classical situation, we would need to re-train the network to compute new optimal parameters. Here, we use Algorithm 1, arising from the adjoint calculus in Section 3.4, with a fixed step size $\gamma = 2$ in order to update the weight and the bias. In Figure 8 we show the solution of the mean field neural network model at $t = 5$ for different number of gradient steps. At each of these steps we get a weight and bias, which is indicated in the title of each plot. After three step of the forward algorithm we obtain new parameters which are able to drive the solution of the mean field equation towards the new target, even starting from the same input data. This example shows how the forward algorithm can be used in order to update weights and bias in case of perturbations in the initial input distribution or in the target distribution.

5.4 Fokker-Planck Type Interpretation of a Neural Network

In this section we aim to validate the results of Section 4.1.1 on a typical example. In particular, the goal is to show that it is possible to fit a standard normal Gaussian distribution, which is taken as target distribution, under the conditions on parameters, activation and diffusion function stated in Section 4.1.1. Here, we consider uniform distribution on $[-1, -\frac{1}{2}]$ as initial condition of the Fokker-Planck type model (21) and evolve it in time. As presented in Section 4.1.1 the Fokker-Planck type interpretation of the neural network is able to fit the Gaussian distribution in the steady state if we choose the identity as activation function, any $w_\infty < 0$, $b_\infty = 0$ and $K(x) = 1$. This approach allows us to drive any initial input to the given target under this choices.

Recall that, on the contrary, and as proven in Section 3.3, the mean field neural network can perform in the case of a hyperbolic tangent or identity activation function only clustering tasks if the conditions $w_\infty < 0$, $b_\infty = 0$ are verified. This means that for large times the distribution approaches a Dirac delta distribution and consequently it is not possible to fit a Gaussian distributed target by using the deterministic SimResNet model. In this perspective, stochastic neural network with stochastic output layers, resulting in a Fokker-Planck kinetic interpretation, allows to fit more general target distributions under the same conditions.

The solution of the Fokker-Planck neural network model for different time steps is presented in Figure 9 showing the convergence to the given target.

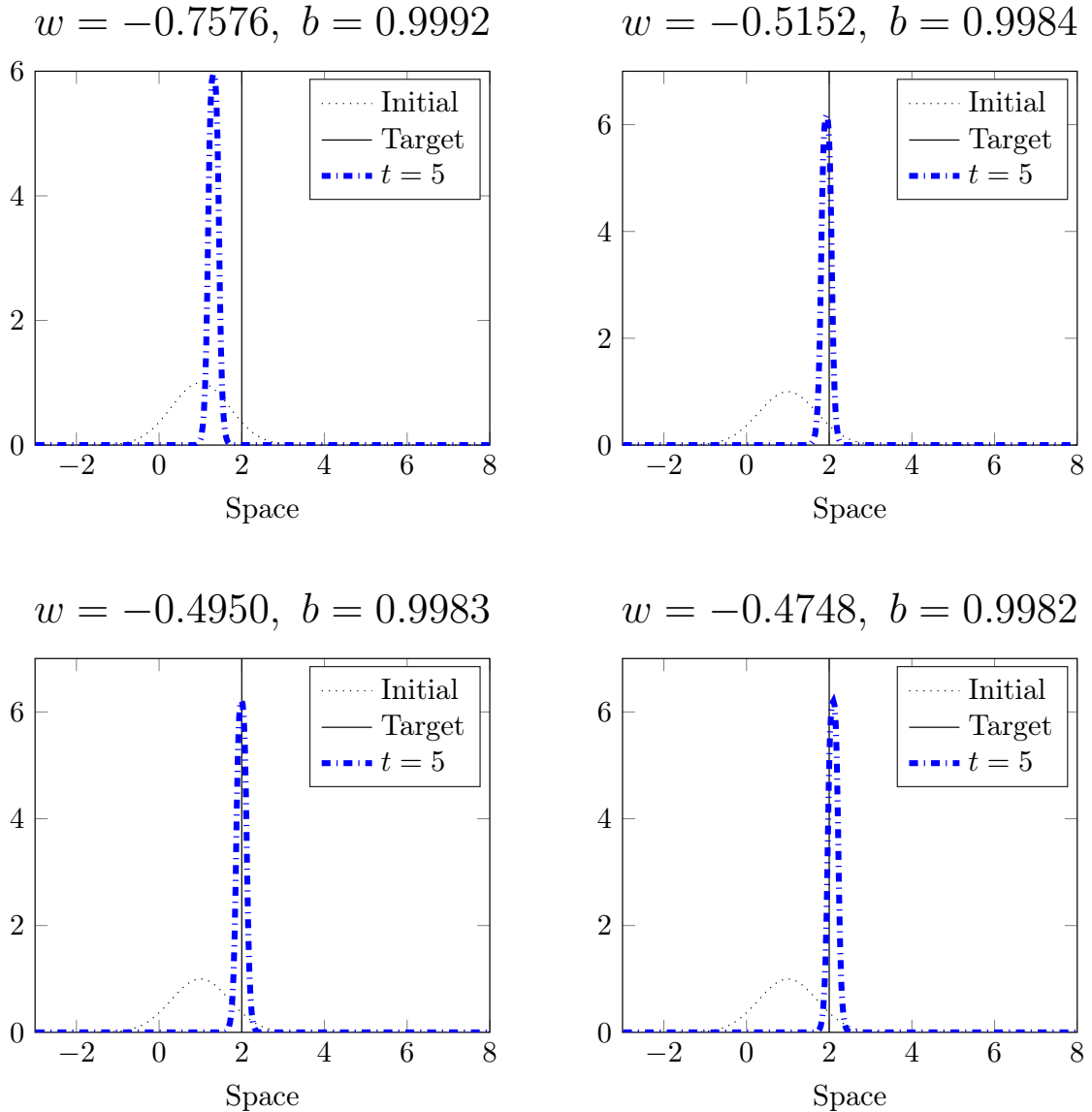


Figure 8: Results of the mean field neural network model with updated weights and bias in the case of a novel target.

6 Conclusion

Starting from the classical formulation of a residual neural network, we have considered a simplified residual neural network which consists in the assumption of one neuron per layer. The effectiveness of this structure has been demonstrated in previous works. By interpreting the discrete structure provided by the layers as a fictitious time discretization, we have derived the corresponding time continuous limit which in turn has led to compute the mean field limit in the number of measurements. Thus, we have switched from a microscopic perspective on the level of time and input data to a probabilistic interpretation provided by the kinetic limit.

The resulting mean field equation has been analyzed in terms of existence of solutions and characterization of steady states. Furthermore, under some assumptions as considering an identity activation function, we have analyzed moment model properties. We have investigated the sensitivity of the loss function with respect to the weight and bias which has allowed to deter-

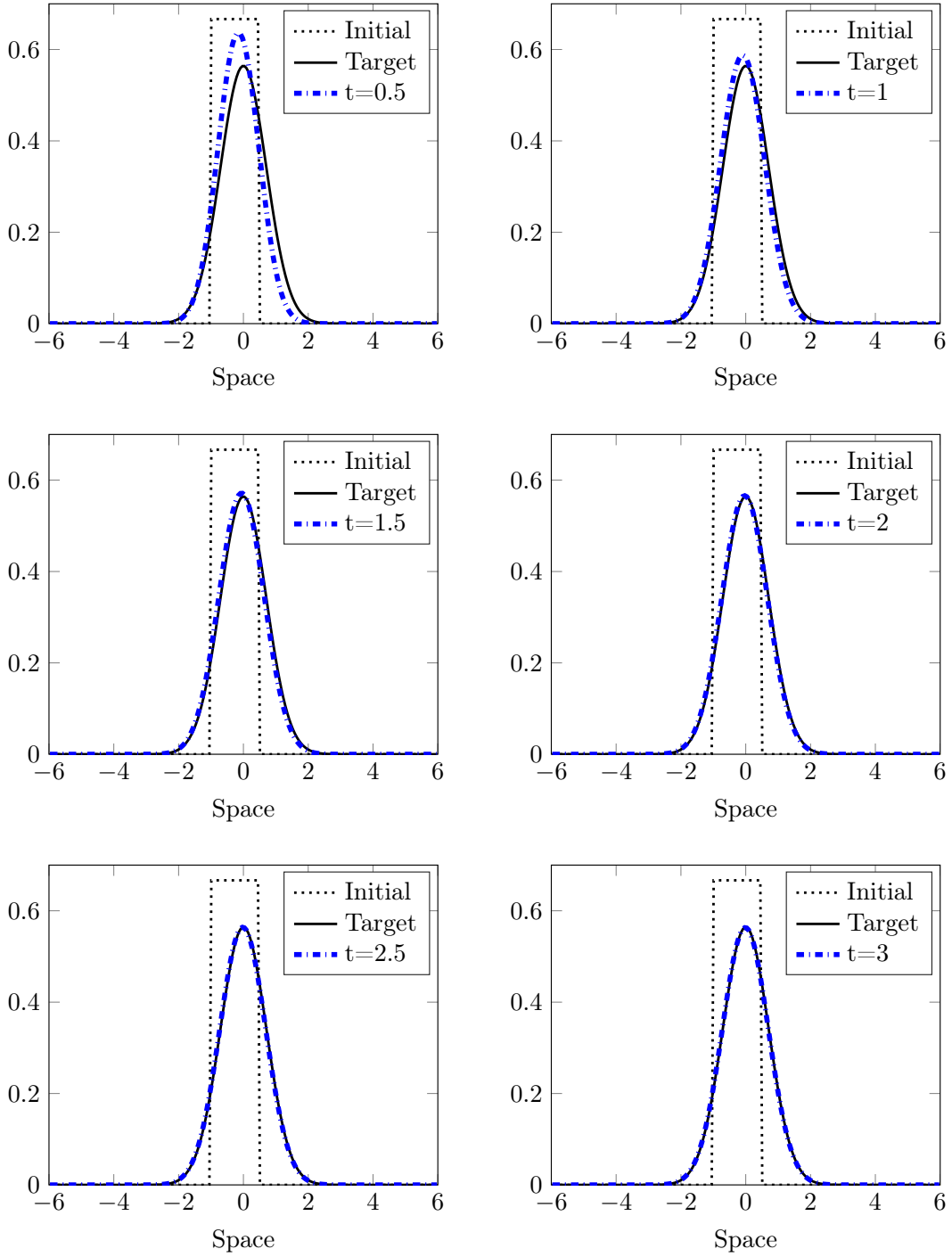


Figure 9: Solution of the Fokker-Planck neural network model at different times. Here, we have chosen the identity as activation function with weight $w = -1$, bias $b = 0$ and diffusion function $K(x) = 1$.

mine a forward algorithm for the parameter update when a change of the input or of the target distribution is introduced, avoiding re-training of the network via back-propagation algorithms.

Finally, we have derived a Boltzmann description of the simplified residual neural network and extended it to the case of a noisy setting, motivated by stochastic residual neural networks with stochastic layers. As consequence, non trivial steady states have been obtained for the limiting Fokker-Planck type model. In the last section we have validated our analysis and have presented simple machine learning applications, namely regression and classification problems.

Acknowledgments

This research is funded by the Deutsche Forschungsgemeinschaft (DFG, German Research Foundation) under Germany's Excellence Strategy – EXC-2023 Internet of Production – 390621612 and supported also by DFG HE5386/15.

M. Herty and T. Trimborn acknowledge the support by the ERS Prep Fund - Simulation and Data Science. The work was partially funded by the Excellence Initiative of the German federal and state governments.

References

- [1] D. Araújo, R. I. Oliveira, and D. Yukimura. A mean-field limit for certain deep neural networks. *arXiv preprint arXiv:1906.00193*, 2019.
- [2] J. A. Carrillo, M. Fornasier, G. Toscani, and F. Vecil. *Mathematical Modeling of Collective Behavior in Socio-Economic and Life Sciences*, chapter Particle, kinetic, and hydrodynamic models of swarming, pages 297–336. Modeling and Simulation in Science, Engineering and Technology. Birkhäuser Boston, 2010.
- [3] T. Q. Chen, Y. Rubanova, J. Bettencourt, and D. K. Duvenaud. Neural ordinary differential equations. In *Advances in neural information processing systems*, pages 6571–6583, 2018.
- [4] R. M. Colombo, M. Mercier, and M. D. Rosini. Stability and total variation estimates on general scalar balance laws. *Commun. Math. Sci.*, 7(1):37–65, 2009.
- [5] I. Cravero, G. Puppo, M. Semplice, and G. Visconti. CWENO: uniformly accurate reconstructions for balance laws. *Math. Comp.*, 87(312):1689–1719, 2018.
- [6] G. Dimarco and G. Toscani. Kinetic modeling of alcohol consumption. *J. Stat. Phys.*, 177:1022–1042, 2019.
- [7] H. I. Fawaz, G. Forestier, J. Weber, L. Idoumghar, and P.-A. Muller. Data augmentation using synthetic data for time series classification with deep residual networks. *arXiv preprint arXiv:1808.02455*, 2018.
- [8] C. Gebhardt, T. Trimborn, F. Weber, A. Bezold, C. Broeckmann, and M. Herty. Simplified ResNet approach for data driven prediction of microstructure-fatigue relationship. *Mechanics of Materials*, 151:103625, 2020.
- [9] J. Goldberger and E. Ben-Reuven. Training deep neural-networks using a noise adaptation layer. In *ICLR*, 2017.
- [10] F. Golse. On the dynamics of large particle systems in the mean field limit. In *Macroscopic and large scale phenomena: coarse graining, mean field limits and ergodicity*, pages 1–144. Springer, 2016.
- [11] E. Haber, F. Lucka, and L. Ruthotto. Never look back - A modified EnKF method and its application to the training of neural networks without back propagation. Preprint arXiv:1805.08034, 2018.
- [12] K. He, X. Zhang, S. Ren, and J. Sun. Deep residual learning for image recognition. *2016 IEEE Conference on Computer Vision and Pattern Recognition (CVPR)*, pages 770–778, 2015.

- [13] P.-E. Jabin. A review of the mean field limits for vlasov equations. *Kinetic & Related Models*, 7(4):661–711, 2014.
- [14] K. Janocha and W. M. Czarnecki. On loss functions for deep neural networks in classification. *Schedae Informaticae*, 2016(Volume 25), 2017.
- [15] G.-S. Jiang and C.-W. Shu. Efficient implementation of weighted ENO schemes. *J. Comput. Phys.*, 126:202–228, 1996.
- [16] M. I. Jordan and T. M. Mitchell. Machine learning: Trends, perspectives, and prospects. *Science*, 349(6245):255–260, 2015.
- [17] A. V. Joshi. *Machine Learning and Artificial Intelligence*. Springer, 2019.
- [18] N. B. Kovachki and A. M. Stuart. Ensemble Kalman inversion: a derivative-free technique for machine learning tasks. *Inverse Probl.*, 35(9):095005, 2019.
- [19] A. Kurganov and D. Levy. A third-order semidiscrete central scheme for conservation laws and convection-diffusion equations. *SIAM J. Sci. Comput.*, 22(4):1461–1488, 2000.
- [20] D. Levy, G. Puppo, and G. Russo. Compact central WENO schemes for multidimensional conservation laws. *SIAM J. Sci. Comput.*, 22(2):656–672, 2000.
- [21] H. Lin and S. Jegelka. Resnet with one-neuron hidden layers is a universal approximator. NIPS’18, page 6172–6181, Red Hook, NY, USA, 2018. Curran Associates Inc.
- [22] Y. Lu, A. Zhong, Q. Li, and B. Dong. Beyond finite layer neural networks: Bridging deep architectures and numerical differential equations. In J. Dy and A. Krause, editors, *35th International Conference on Machine Learning, ICML 2018*, 35th International Conference on Machine Learning, ICML 2018, pages 5181–5190. International Machine Learning Society (IMLS), 2018. 35th International Conference on Machine Learning, ICML 2018 ; Conference date: 10-07-2018 Through 15-07-2018.
- [23] S. Mei, A. Montanari, and P.-M. Nguyen. A mean field view of the landscape of two-layer neural networks. *Proceedings of the National Academy of Sciences*, 115(33):E7665–E7671, 2018.
- [24] S. Mishra. A machine learning framework for data driven acceleration of computations of differential equations. *Math. Eng.*, 1(1):118–146, 2019.
- [25] V. C. Müller and N. Bostrom. Future progress in artificial intelligence: a survey of expert opinion. In *Fundamental issues of artificial intelligence*, volume 376 of *Synth. Libr.*, pages 553–570. Springer, [Cham], 2016.
- [26] H. Noh, T. You, J. Mun, and B. Han. Regularizing deep neural networks by noise: Its interpretation and optimization. In I. Guyon, U. V. Luxburg, S. Bengio, H. Wallach, R. Fergus, S. Vishwanathan, and R. Garnett, editors, *Advances in Neural Information Processing Systems 30*, pages 5109–5118. Curran Associates, Inc., 2017.
- [27] S. C. Onar, A. Ustundag, Ç. Kadaifci, and B. Oztaysi. The changing role of engineering education in industry 4.0 era. In *Industry 4.0: Managing The Digital Transformation*, pages 137–151. Springer, 2018.
- [28] F. Otto and C. Villani. Generalization of an inequality by talagrand and links with the logarithmic sobolev inequality. *Journal of Functional Analysis*, 173(2):361–400, 2000.
- [29] L. Pareschi and G. Toscani. Self-Similarity and Power-Like Tails in Nonconservative Kinetic Models. *J. Stat. Phys.*, 124(2-4):747–779, 2006.

- [30] L. Pareschi and G. Toscani. *Interacting Multiagent Systems. Kinetic equations and Monte Carlo methods*. Oxford University Press, 2013.
- [31] D. Ray and J. S. Hesthaven. An artificial neural network as a troubled-cell indicator. *J. Comput. Phys.*, 367(15):166–191, 2018.
- [32] D. Ray and J. S. Hesthaven. Detecting troubled-cells on two-dimensional unstructured grids using a neural network. *J. Comput. Phys.*, 397, 2019. To appear.
- [33] L. Ruthotto and E. Haber. Deep neural networks motivated by partial differential equations. *J. Math. Imaging Vis.*, 62:352–364, 2020.
- [34] L. Ruthotto, S. Osher, W. Li, L. Nurbekyan, and S. W. Fung. A machine learning framework for solving high-dimensional mean field game and mean field control problems. *Proceedings of the National Academy of Sciences*, 117:9183 – 9193, 2020.
- [35] R. Schmitt and G. Schuh. *Advances in Production Research: Proceedings of the 8th Congress of the German Academic Association for Production Technology (WGP), Aachen, November 19-20, 2018*. Springer, 2018.
- [36] J. Sirignano and K. Spiliopoulos. Mean field analysis of neural networks: A central limit theorem. *Stochastic Processes and their Applications*, 2019.
- [37] H. Tercan, T. Al Khawli, U. Eppelt, C. Büscher, T. Meisen, and S. Jeschke. Improving the laser cutting process design by machine learning techniques. *Production Engineering*, 11(2):195–203, 2017.
- [38] G. Toscani. Kinetic models of opinion formation. *Commun. Math. Sci.*, 3(4):481–496, 2006.
- [39] D. Tran, M. W. Dusenberry, M. V. D. Wilk, and D. Hafner. Bayesian layers: A module for neural network uncertainty. In *NeurIPS*, 2019.
- [40] T. Trimborn, S. Gerster, and G. Visconti. Spectral methods to study the robustness of residual neural networks with infinite layers. *Foundations of Data Science*, 2(3):257–278, 2020.
- [41] Q. Wang, J. S. Hesthaven, and D. Ray. Non-intrusive reduced order modelling of unsteady flows using artificial neural networks with application to a combustion problem. *J. Comput. Phys.*, 384:289–307, 2019.
- [42] K. Watanabe and S. G. Tzafestas. Learning algorithms for neural networks with the Kalman filters. *J. Intell. Robot. Syst.*, 3(4):305–319, 1990.
- [43] P. J. Werbos. *The roots of backpropagation: from ordered derivatives to neural networks and political forecasting*, volume 1. John Wiley & Sons, 1994.
- [44] M. Wooldridge. Artificial Intelligence requires more than deep learning - but what, exactly? *Artificial Intelligence*, 289:103386, 2020.
- [45] Z. Wu, C. Shen, and A. Van Den Hengel. Wider or deeper: Revisiting the resnet model for visual recognition. *Pattern Recognition*, 90:119–133, 2019.
- [46] A. Yegenoglu, S. Diaz, K. Krajsek, and M. Herty. Ensemble Kalman filter optimizing deep neural networks. In *Conference on Machine Learning, Optimization and Data Science*, volume 12514. Springer LNCS Proceedings, 2020.
- [47] Z. You, J. Ye, K. Li, Z. Xu, and P. Wang. Adversarial noise layer: Regularize neural network by adding noise. In *2019 IEEE International Conference on Image Processing, ICIP 2019, Taipei, Taiwan, September 22-25, 2019*, pages 909–913. IEEE, 2019.

- [48] A. Zeng, S. Song, K.-T. Yu, E. Donlon, F. R. Hogan, M. Bauza, D. Ma, O. Taylor, M. Liu, E. Romo, et al. Robotic pick-and-place of novel objects in clutter with multi-affordance grasping and cross-domain image matching. In *2018 IEEE International Conference on Robotics and Automation (ICRA)*, pages 1–8. IEEE, 2018.
- [49] D. Zhang, L. Guo, and G. E. Karniadakis. Learning in modal space: solving time-dependent stochastic PDEs using physics-informed neural networks. *SIAM J. Sci. Comput.*, 42(2):A639–A665, 2020.